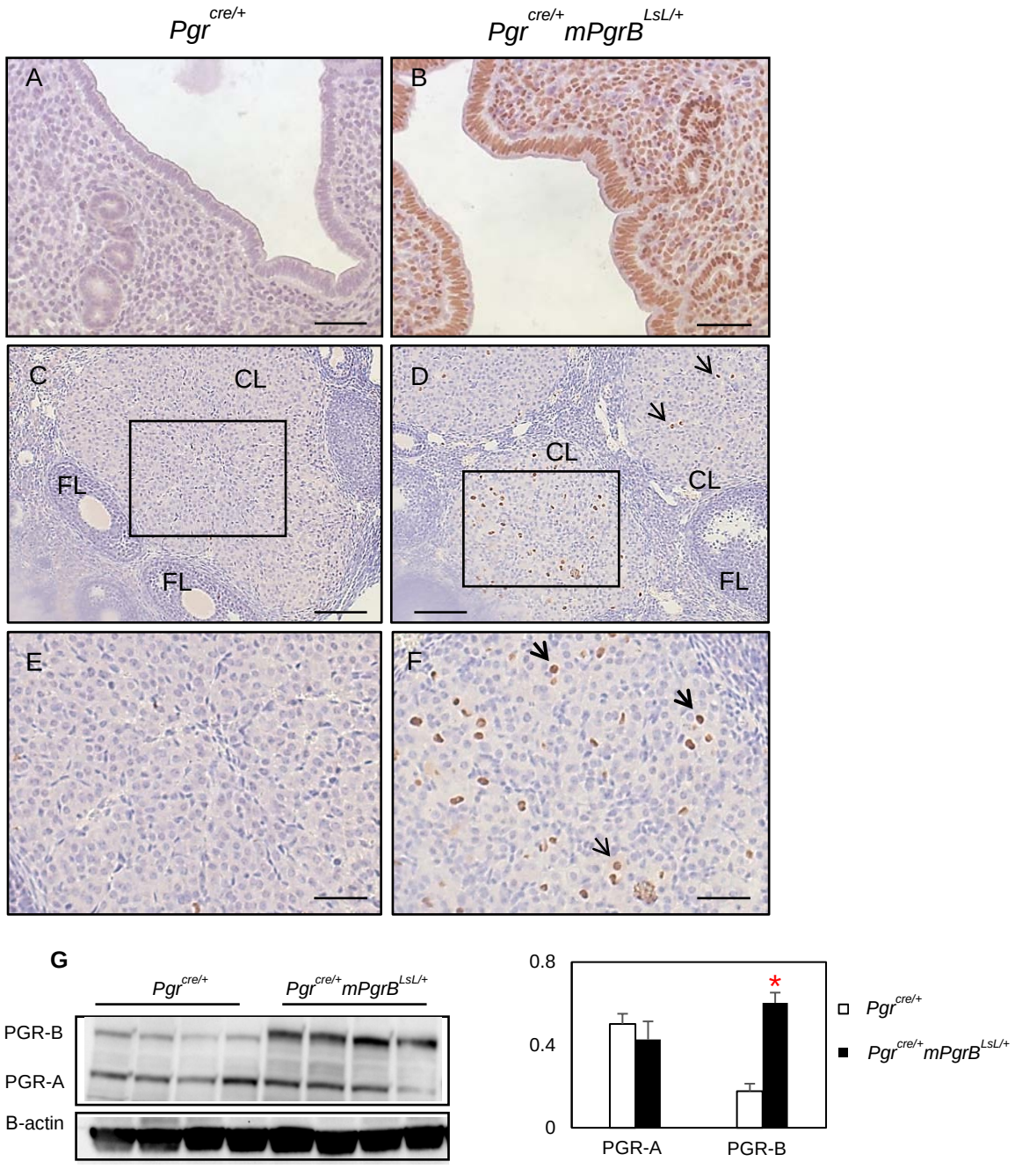

Supplemental Figure 1: Levels of the conditional overexpression allele for *mPgrB* in uterine and ovarian tissue. (A-D) Myc-tag immunohistochemistry of 8-week-old wildtype uterus (A) and ovary (C) compared to $Pgr^{cre/+}mPgrB^{LsL/+}$ mouse uterus (B) and ovary (D). (E-F) High magnification images of corpora lutea from insets in (C-D) in wildtype ovary (E) and $Pgr^{cre/+}mPgrB^{LsL/+}$ ovary (F). (G) Western blot and the associated quantification of PGR levels from whole uterine isolates in wildtype $Pgr^{cre/+}$ and $Pgr^{cre/+}mPgrB^{LsL/+}$ mice. PGRB protein (118 kDa), PGRA protein (90 kDa). C-D 100 µM scale bar, A-B, E-F 50 µM scale bar. n=2-4 mice for immunohistochemistry. Each band of the western blot indicates one mouse. Student's t-test used to compare groups. *p<0.05 compared to $Pgr^{cre/+}$. Scale bar means SEM.

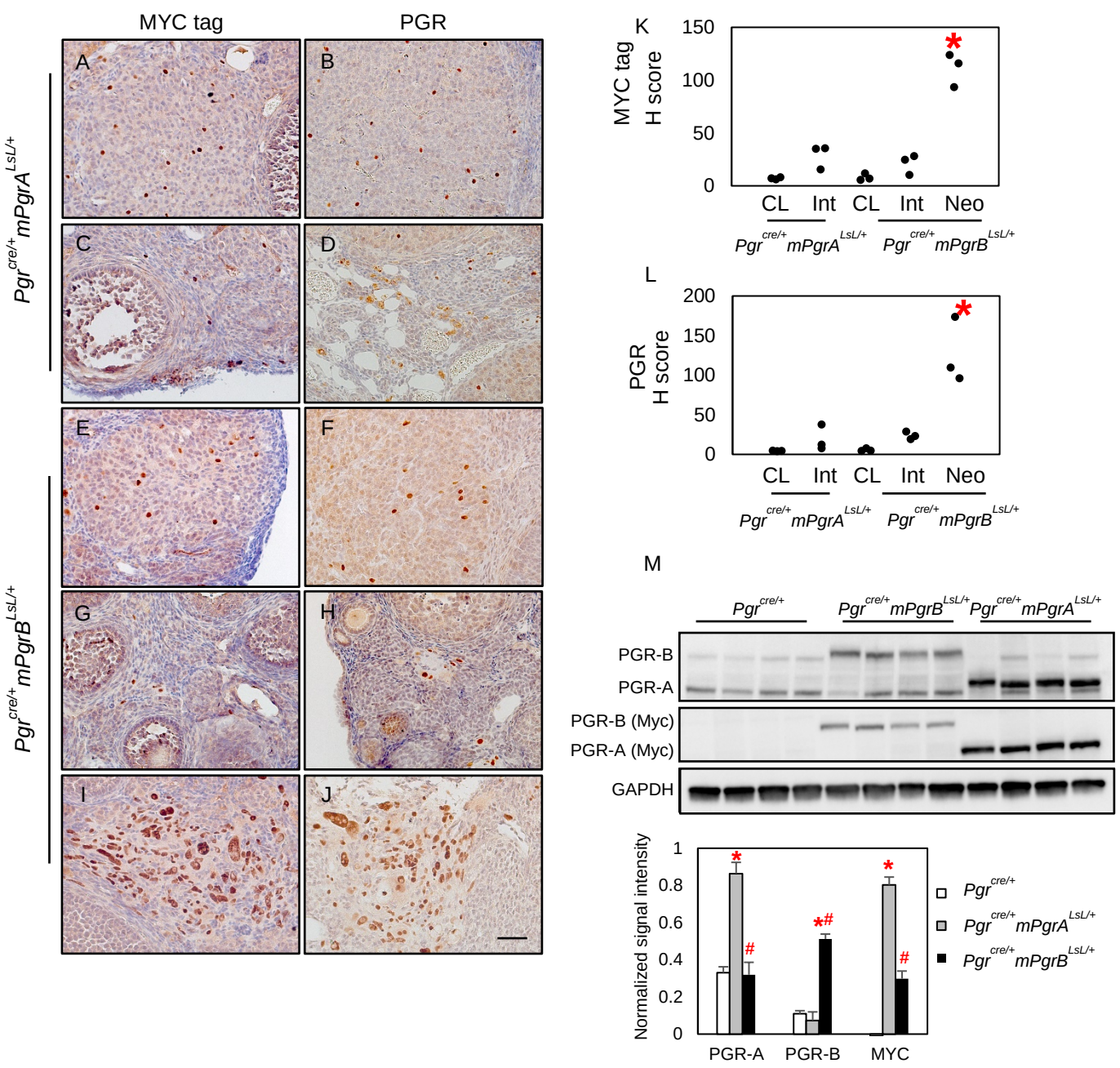

Supplemental Figure 2: PGR transgene levels are comparable in both *Pgr*$^{cre/+}$*mPgrA*$^{LsL/+}$ and *Pgr*$^{cre/+}$*mPgrB*$^{LsL/+}$ mice at 13 weeks of age. Immunohistochemistry showed MYC tag staining (A, C, E, G, I) and PGR (B, D, F, H, J) in the CL (A, B) and Int (C, D) of *Pgr*$^{cre/+}$*mPgrA*$^{LsL/+}$ ovary (A-D), the CL (E, F) and Int (G, H), and Neoplastic tumor (I, J) of *Pgr*$^{cre/+}$*mPgrB*$^{LsL/+}$ ovary (E-J). n=3 mice. *p<0.05. CL: Corpus luteum; Int: Interstitial tissues; Neo: 23 week neoplastic stage tumor. H score indices for MYC tag (K) and PGR (L) immunohistochemistry. Western blot of PGR and MYC tag and the associated quantification in whole uterine isolates (M). One-way ANOVA with post hoc Tukey's test was used to compare groups. *p<0.05 compared with *Pgr*$^{cre/+}$ mice. #p<0.05 compared with *Pgr*$^{cre/+}$*mPgrA*$^{LsL/+}$ mice. 50 µM scale bar. n=3 mice for immunohistochemistry. n=4 mice for western blot. Scale bar means SEM.

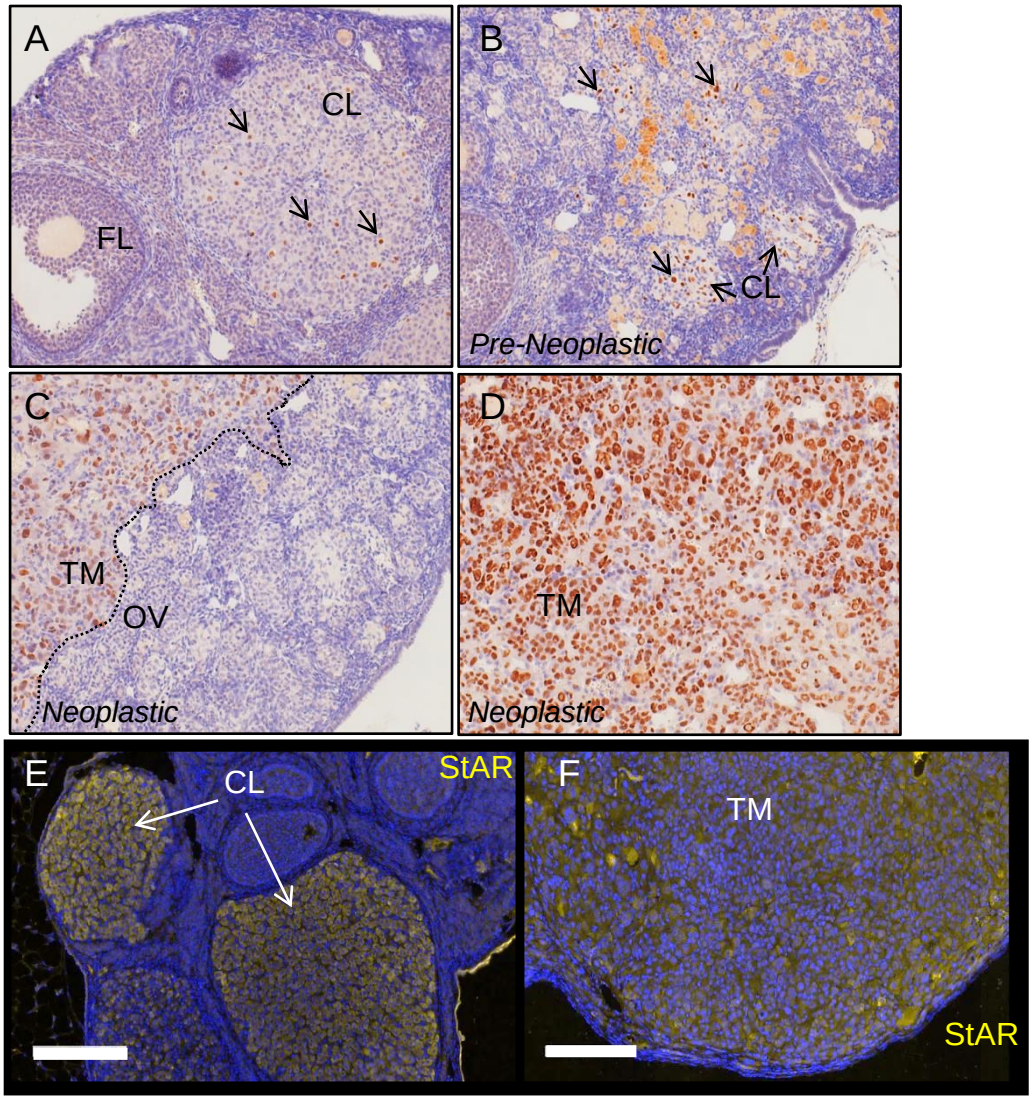

Supplemental Figure 3: PGR positive ovarian neoplasia from $Pgr^{cre/+}mPgrB^{LsL/+}$ mice consume the entire ovarian bursa and exhibit robust StAR expression levels. Immunohistochemical images of PGR positive cells within corpora lutea (indicated by arrows) from normal $Pgr^{cre/+}mPgrB^{LsL/+}$ mouse ovaries at 10 weeks (A) and from pre-neoplastic ovaries (B). (C-D) PGR immunohistochemistry of PGR positive outgrowth of cells occurring in neoplastic ovaries from $Pgr^{cre/+}mPgrB^{LsL/+}$ mice. Immunofluorescent staining for steroidogenic acute regulatory protein (StAR) in a wildtype ovary (E) and neoplastic ovarian tumor (F) of $Pgr^{cre/+}mPgrB^{LsL/+}$ mice. Blue staining is DAPI, yellow staining represents positive StAR staining. 100 µM scale bar for A-D. 200 µM scale bar for E-F. FL=follicle, CL=corpora lutea, OV=ovary, TM=tumor tissue. n=4 mice for A-B images. C-D are representative of individual mouse tumor burden over time. n=3 mice for E-F images.

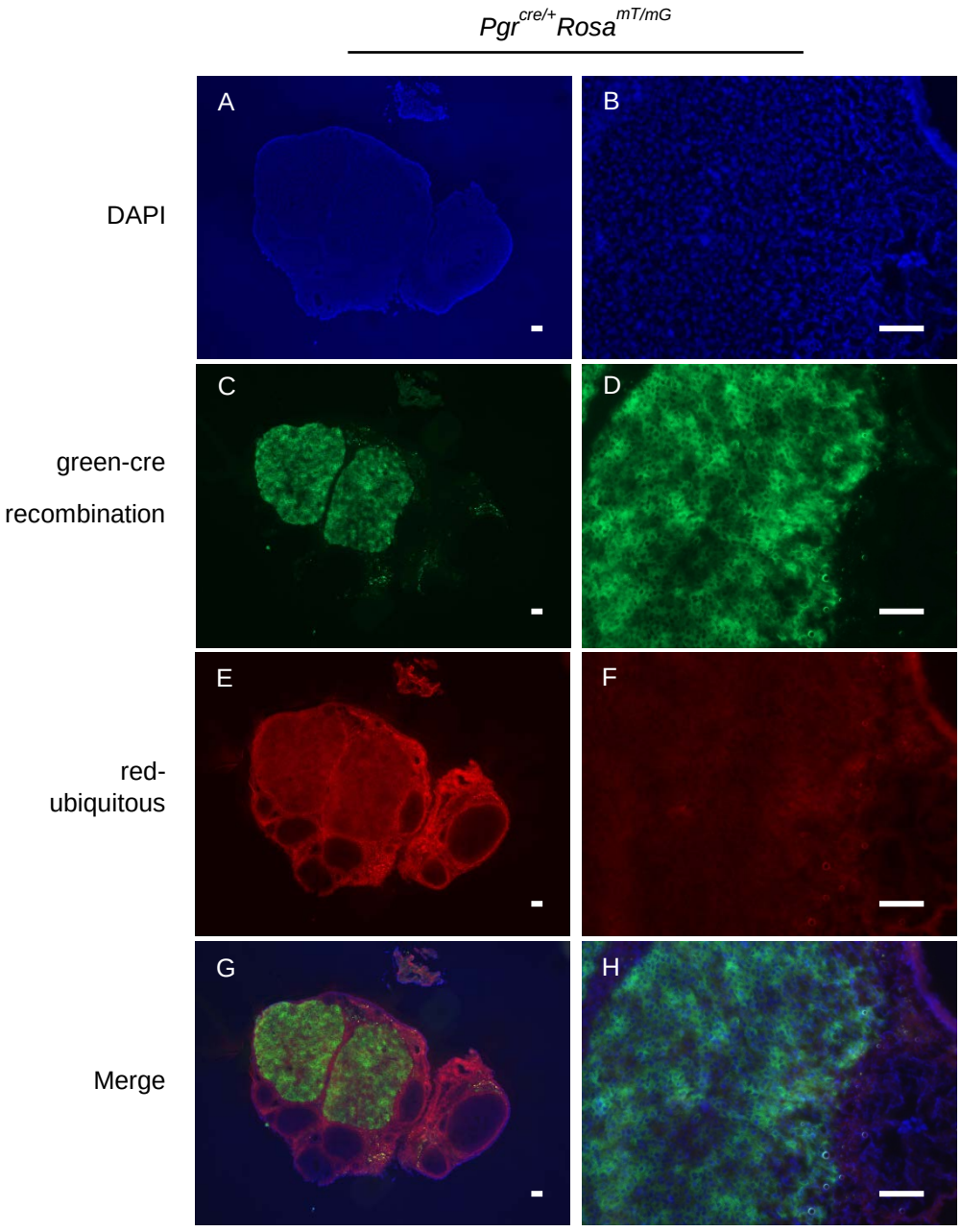

Supplemental Figure 4: Lineage tracing using the *Pgr*$^{cre/+}$*Rosa*$^{mT/mG}$ model demonstrates localized Cre recombination to the corpus luteum at 8 weeks of age. DAPI (A, B), positive Cre recombinase activity in green from the *Rosa*$^{mT/mG}$ construct (C, D), ubiquitous red fluorescence from *Rosa*$^{mT/mG}$ model (E, F), and red-green overlay (G, H). *Pgr*$^{cre/+}$*Rosa*$^{mT/mG}$ mouse ovary (A, C, E, G) and ovarian corpus luteum (B, D, F, H). 100 µM scale bar. n=3 mice.

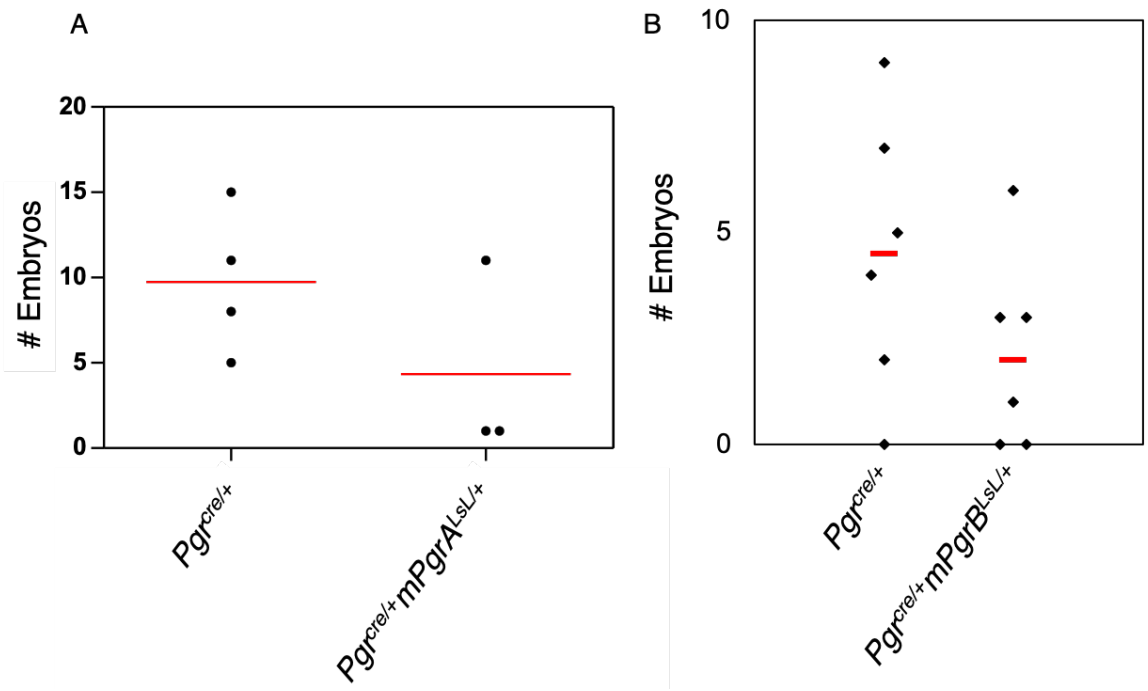

Supplemental Figure 5: PGRA or PGRB expression does not impair ovarian function. (A) Embryos were flushed from the oviduct from super-ovulated and mated *Pgr*$^{cre/+}$*mPgrA*$^{LsL/+}$ females. n=3 mice. (B) Embryos were flushed from the oviduct at Day 1.5 of pregnancy in *Pgr*$^{cre/+}$*mPgrB*$^{LsL/+}$ mice. n=6 mice. Red bars represent the mean. Each dot indicates the number of embryos of one mouse. Student's t-test was utilized to compare data groups.

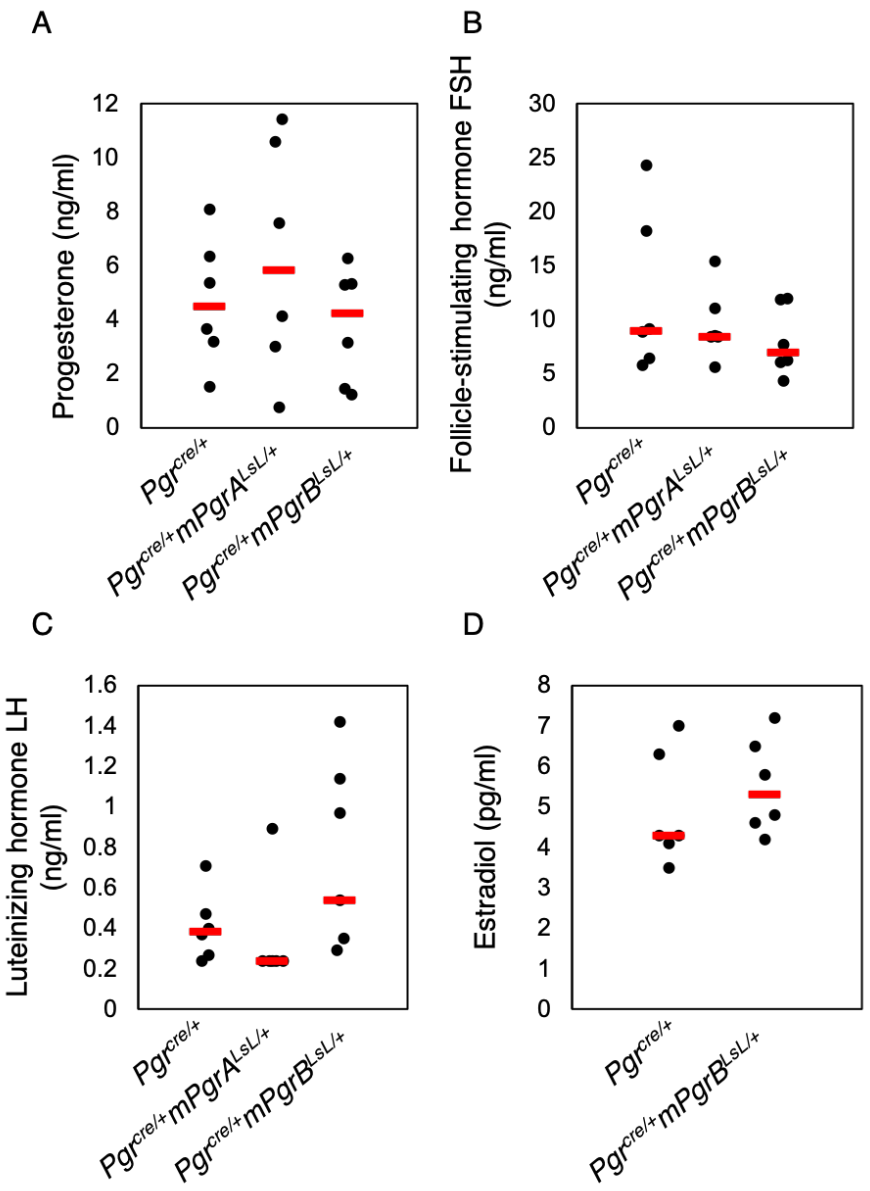

Supplemental Figure 6: Increased ovarian PGR expression does not impair endogenous hormone levels. Serum levels of progesterone (A), follicle-stimulating hormone (FSH) (B), and luteinizing hormone (LH) (C) from 23 week-old $Pgr^{cre/+}mPgrA^{LsL/+}$ mice and $Pgr^{cre/+}mPgrB^{LsL/+}$ mice at diestrous stage. (D) Serum estradiol levels for $Pgr^{cre/+}$ and $Pgr^{cre/+}mPgrB^{LsL/+}$ mice. Each dot indicates the serum level from one mouse. The red line indicates median level. n=6 mice. One-way ANOVA with post-hoc Tukey's test was used for progesterone, FSH, and LH analyses. Student's t-test was utilized to compare estradiol levels.

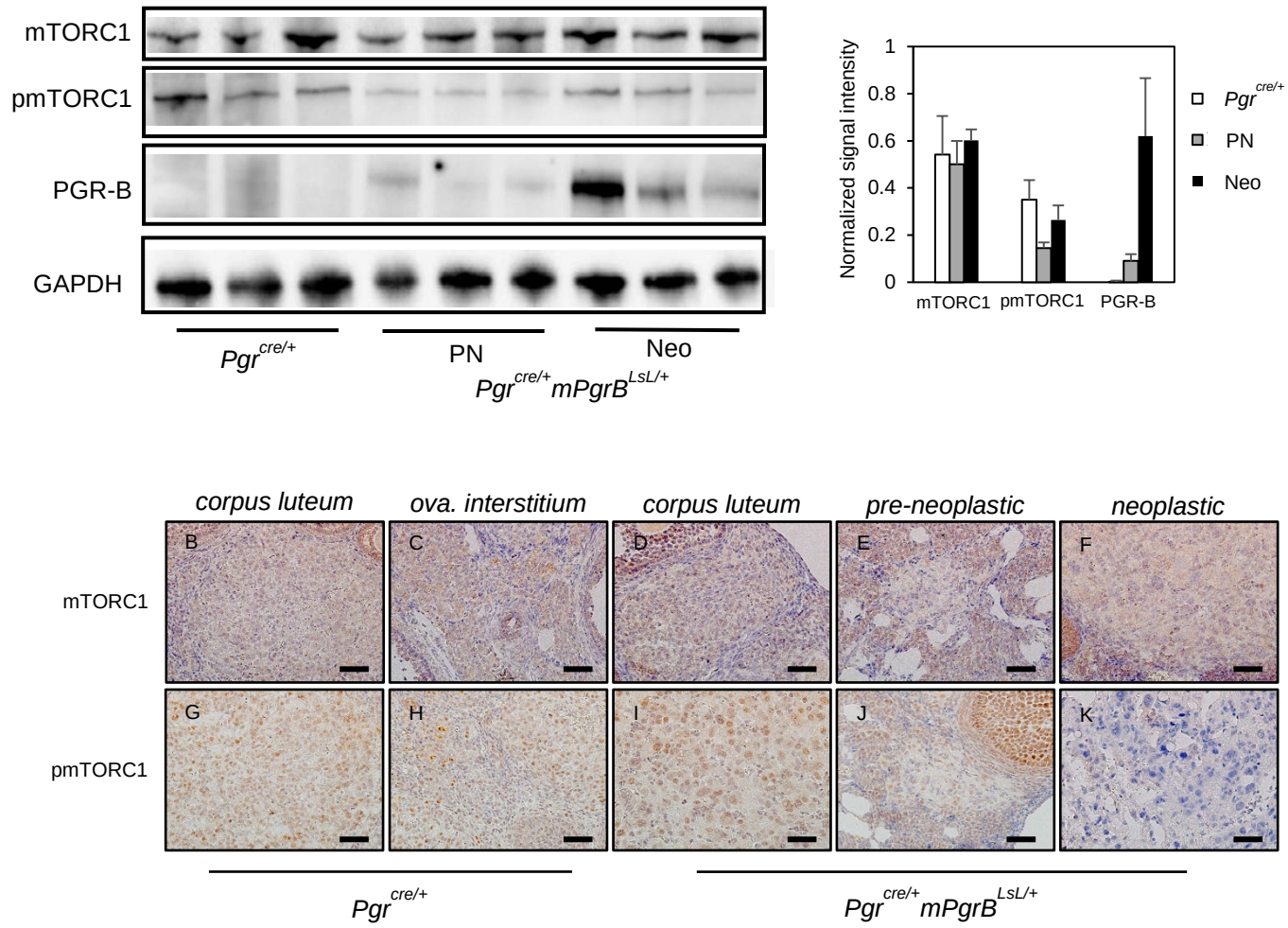

Supplemental Figure 7: Phosphorylated mTORC1 protein levels are slightly reduced in neoplasia of the *Pgr*$^{cre/+}$*mPgrB*$^{LsL/+}$ ovary. Western blot of mTORC1, pmTORC1, PGRB and GAPDH in the *Pgr*$^{cre/+}$, and *Pgr*$^{cre/+}$*mPgrB*$^{LsL/+}$ ovaries at different stages with the associated quantification (A). Immunohistochemistry of mTORC1 (B-F) and pmTORC1 (G-K) staining in the corpus luteum (B, G) and ovarian interstitium (C, H) of the *Pgr*$^{cre/+}$ovary (B, C, G, H), the corpus luteum (D, I), pre-neoplastic (E, J), and neoplastic tumor (F, K) of *Pgr*$^{cre/+}$*mPgrB*$^{LsL/+}$ ovary (D-F, I-K). 50 µM scale bar. n=3 mice. Scale bar means SEM. One-way ANOVA with post-hoc Tukey's test used to determine significance.

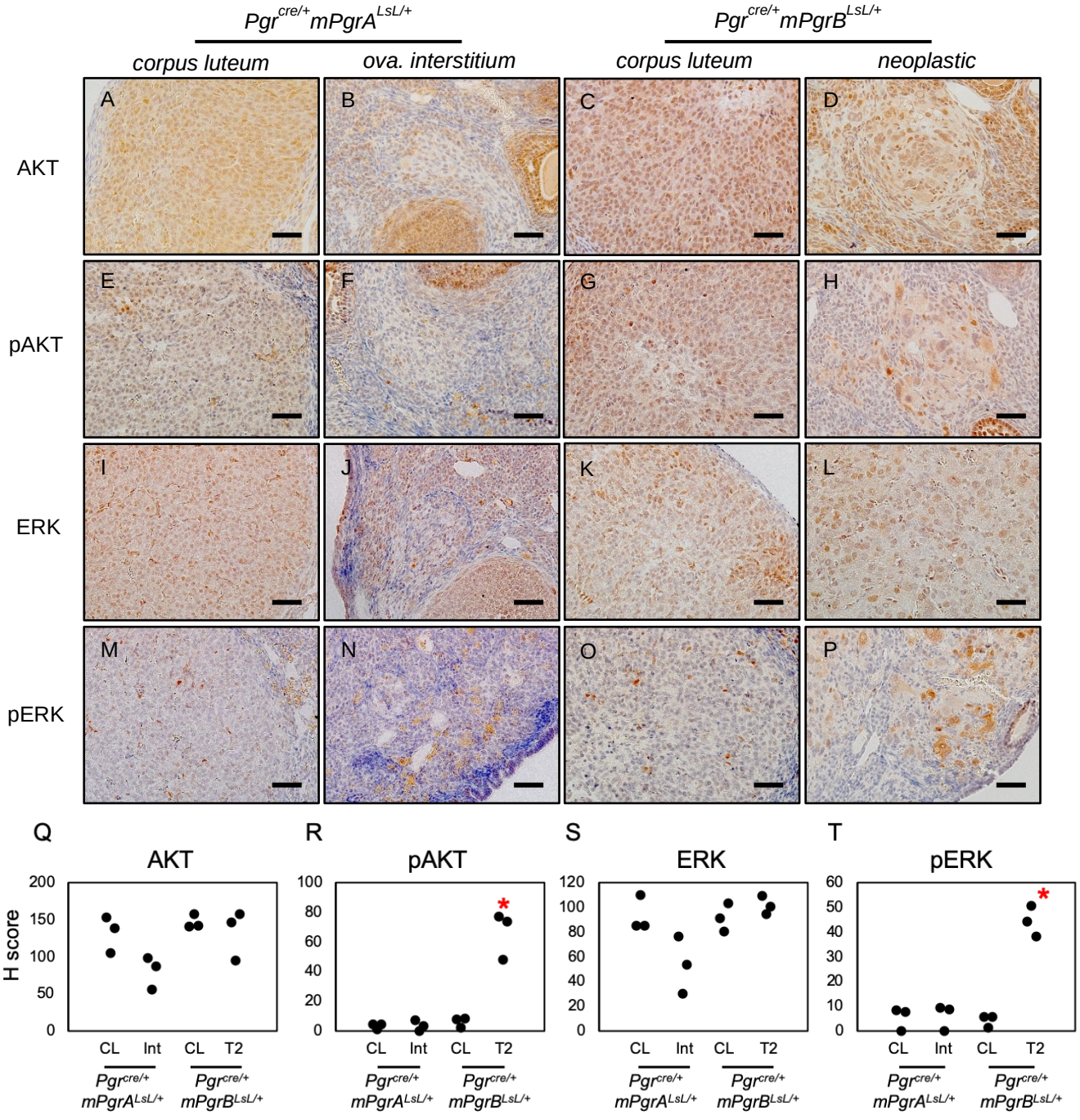

Supplemental Figure 8: pAKT and pERK expression in the $Pgr^{cre/+}mPgrA^{LsL/+}$ ovaries were comparable to the corpus luteum of $Pgr^{cre+}mPgrB^{LsL/+}$ ovary, but much lower than the tumor tissues of $Pgr^{cre/+}mPgrB^{LsL/+}$ ovary at 23 weeks neoplastic. Immunohistochemistry showed AKT (A-D), pAKT (E-H), ERK (I-L) and pERK (M-P) in the CL (A, E, I, M) and Int (B, F, J, N) of $Pgr^{cre+}mPgrA^{LsL/+}$ ovary compared to CL (C, G, K O) and neoplastic ovary (D, H L P) of $Pgr^{cre/+}mPgrB^{LsL/+}$ mice. H score of AKT (Q), pAKT (R), ERK (S) and pERK (T). n=3 mice. CL: Corpus luteum; Int: Interstitial tissues; T2: neoplastic (23wks). One-way ANOVA with post-hoc Tukey's test for significance. *p<0.05 compared to CL. 50 µM scale bar.

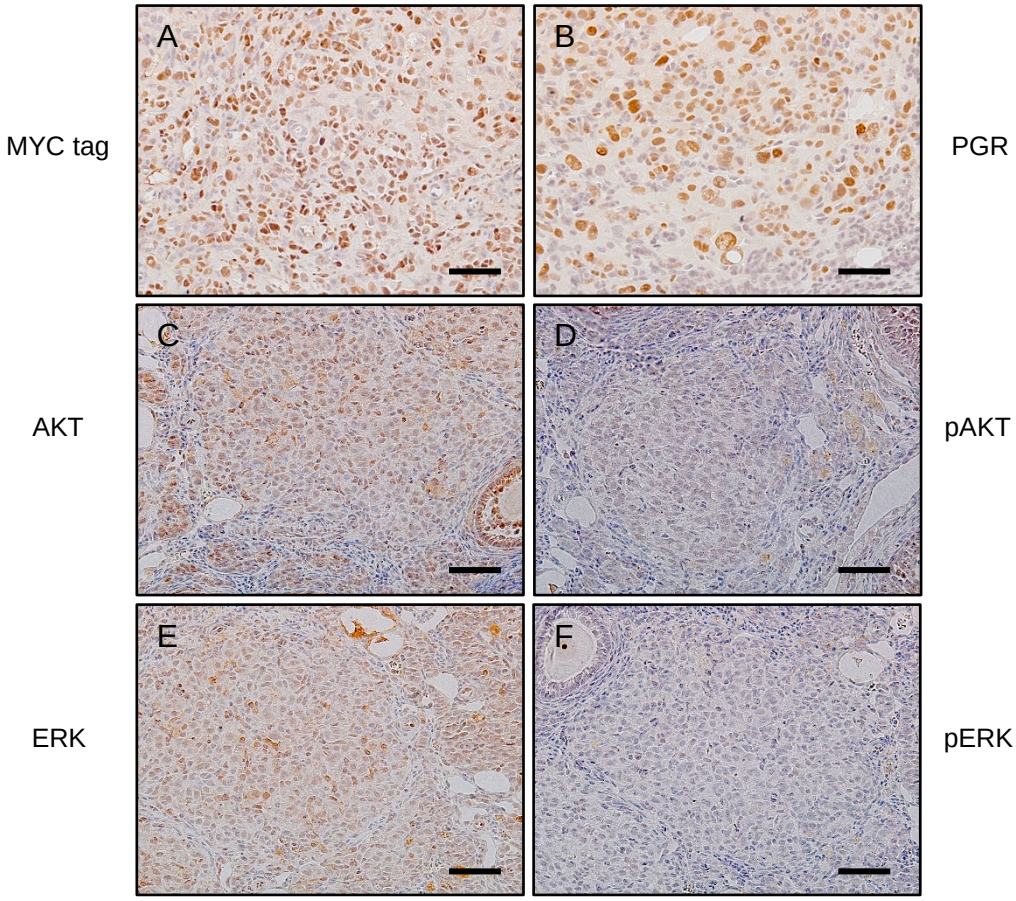

Supplemental Figure 9: pAKT and pERK were not activated in the *Pgr*$^{cre/+}$*mPgrA*$^{LsL/+}$ ovaries with neoplasia. Immunohistochemistry of MYC tagged PGRA (A), PGR (B), AKT (C), pAKT (D), ERK (E) and pERK (F) in the *Pgr*$^{cre/+}$*mPgrA*$^{LsL/+}$ ovary. n=1 mouse. 50 µM scale bar.

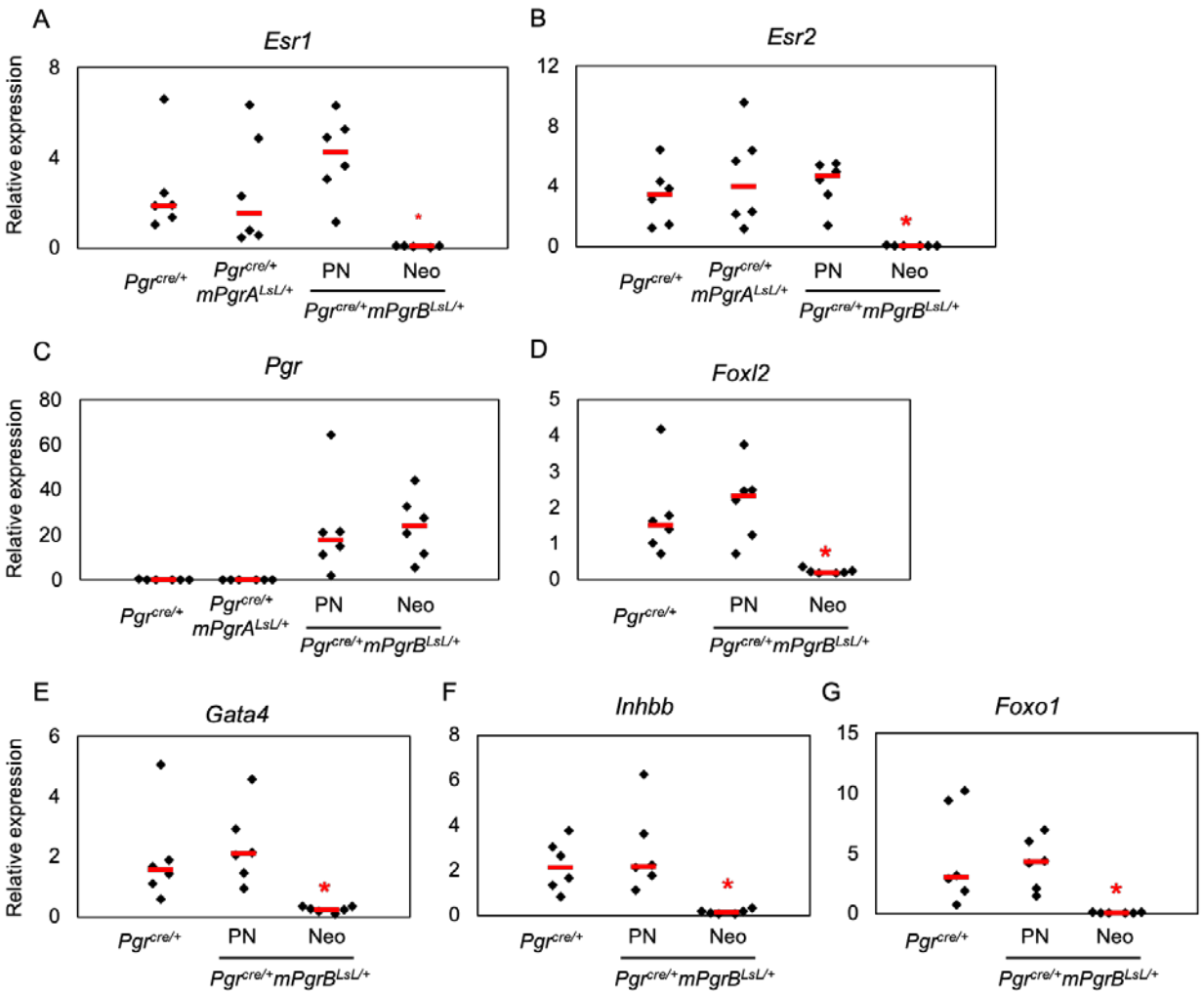

Supplemental Figure 10: Message levels of estrogen and progesterone receptors and granulosa cell markers decrease in advanced PGR-driven neoplasia. Relative message levels for (A) *Esr1*, (B) *Esr2*, (C) *Pgr*, and granulosa cell markers (D) *Foxl2*, (E) *Gata4*, (F) *Inhbb*, and (G) *Foxo1* in $Pgr^{cre/+}$ control ovarian tissue compared to $Pgr^{cre/+}mPgrA^{LsL/+}$ ovaries and $Pgr^{cre/+}mPgrB^{LsL/+}$ pre-neoplastic (PN) and neoplastic (Neo) ovarian tissue. One-way ANOVA with post-hoc Tukey's test used to compare groups. *$p<0.05$ compared to $Pgr^{cre/+}$. n=6 mice.

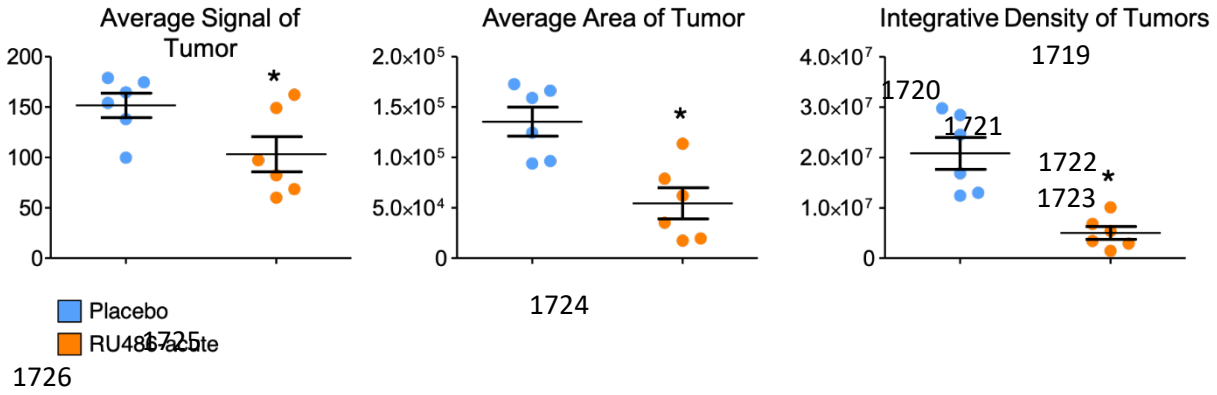

1724

1725

1726

1727

1728 Supplemental Figure 11: *Pgr*$^{cre/+}$*mPgrB*$^{LsL/+}$ tumors exhibit decreased density and size after acute RU486
1729 treatment. (A-C) ImageJ analysis on tumor frames exhibiting the greatest tumor diameter taken from the
1730 final week of treatment. (A) Reports average signal output or lightened areas in tumor images in RU486
1731 vs placebo groups. (B) Depicts average areas of tumor as a function of the measurement tool used in the
1732 ImageJ software platform of RU486 versus placebo treated tumors. (C) Average integrative density (cell
1733 signal multiplied by cell area) for the ultrasound frames from RU486 versus placebo treated
1734 *Pgr*$^{cre/+}$*mPgrB*$^{LsL/+}$ ovarian tumors. Student's t-test utilized to determine significance. *p<0.05. Error bars
1735 represent ±SEM. n=6 mice.
1736
1737
1738
1739
1740
1741
1742
1743
1744
1745
1746
1747
1748
1749
1750
1751
1752
1753
1754
1755
1756
1757
1758
1759
1760
1761
1762

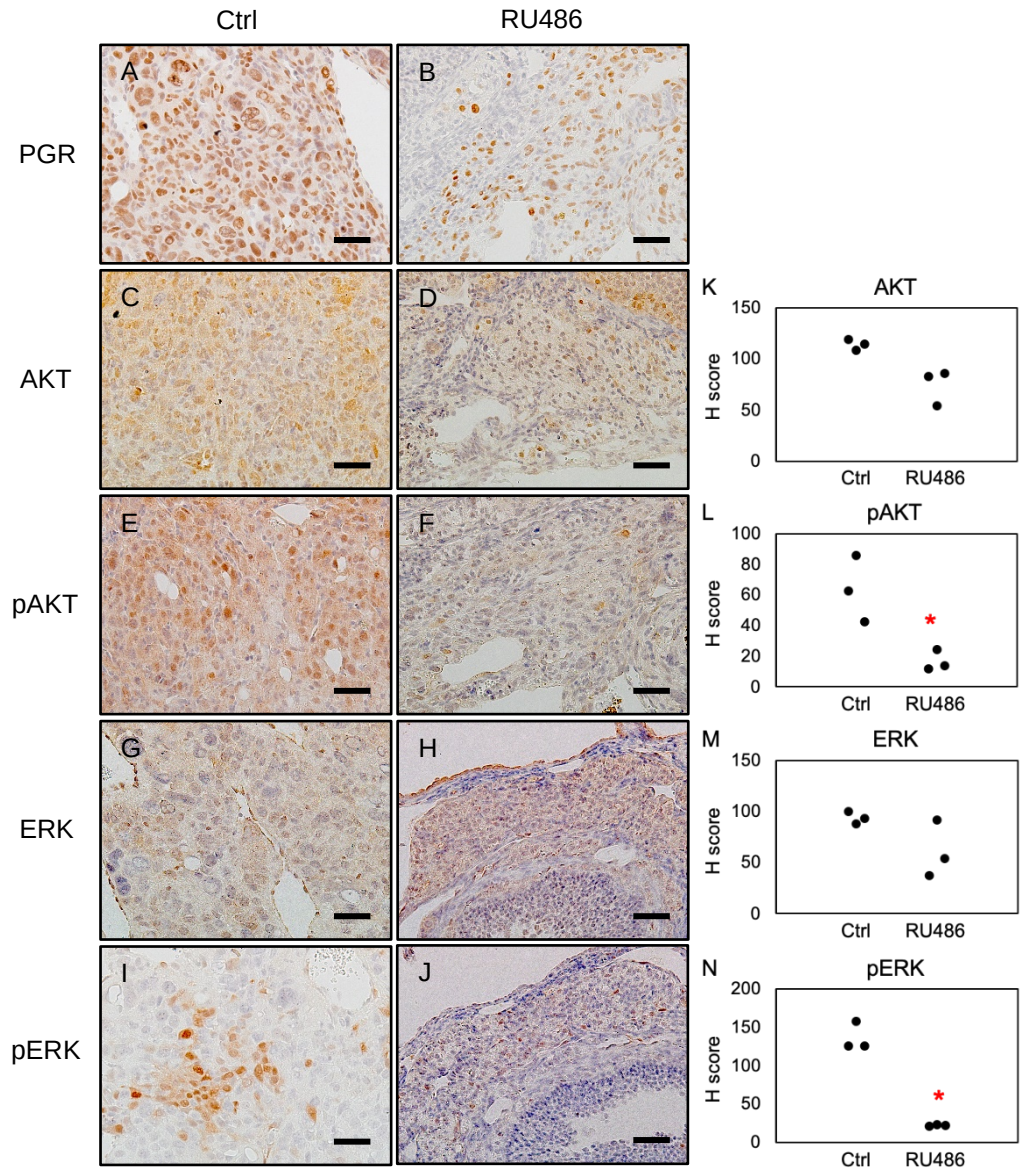

Supplemental Figure 12: Chronic RU486 treatment suppresses pAKT and pERK levels in the *Pgr*$^{cre/+}$*mPgrB*$^{LsL/+}$ ovarian tumor tissue. Immunohistochemistry of PGR (A, B), AKT (C, D), pAKT (E, F), ERK (G, H), and pERK (I, J) in the control (Ctrl) (A, C, E, G, I) and RU486 treated (B, D, F, H, J) *Pgr*$^{cre/+}$*mPgrB*$^{LsL/+}$ ovaries. H score of AKT (K), pAKT (L), ERK (M), and pERK (N). Ctrl: age comparable *Pgr*$^{cre/+}$*mPgrB*$^{LsL/+}$ ovaries without treatment. RU486: RU486 pellet treated. n=3 mice. Student's t-test used to compare groups. *p<0.05. 50 µM scale bar.

A

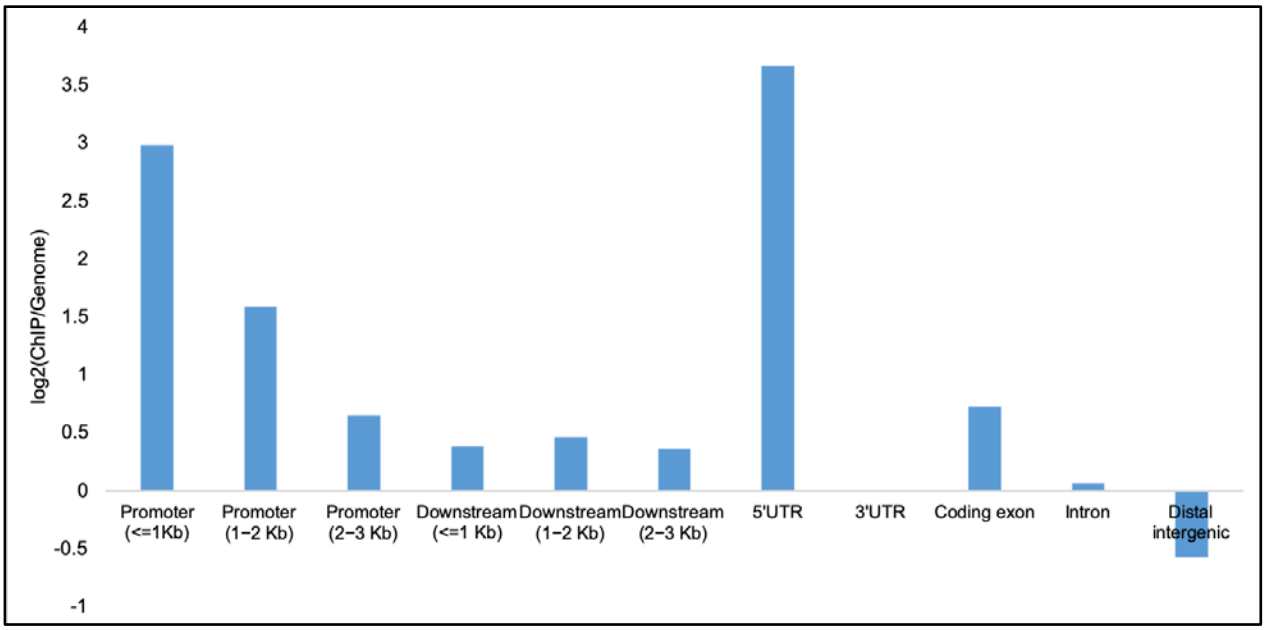

B

1		Nuclear Receptor
2		ATF/JUN
3		GATA
4		CEBP
5		HNF1
6		ETS
7		STAT
8		RUNX
9	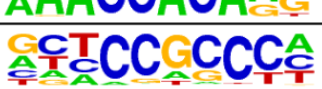	SP1/KLF

Supplemental Figure 13: PGR ChIP-seq is enriched at promoter regions and binds to hormone receptor binding sequences. (A) Enrichment distribution of PGR binding on the genome compared to normal expected enrichment. Data is equivalent to the natural log of PGR chip binding/basal genome binding. (B) Top binding of known motifs by PGR in the ovarian tumor ChIP-Seq.

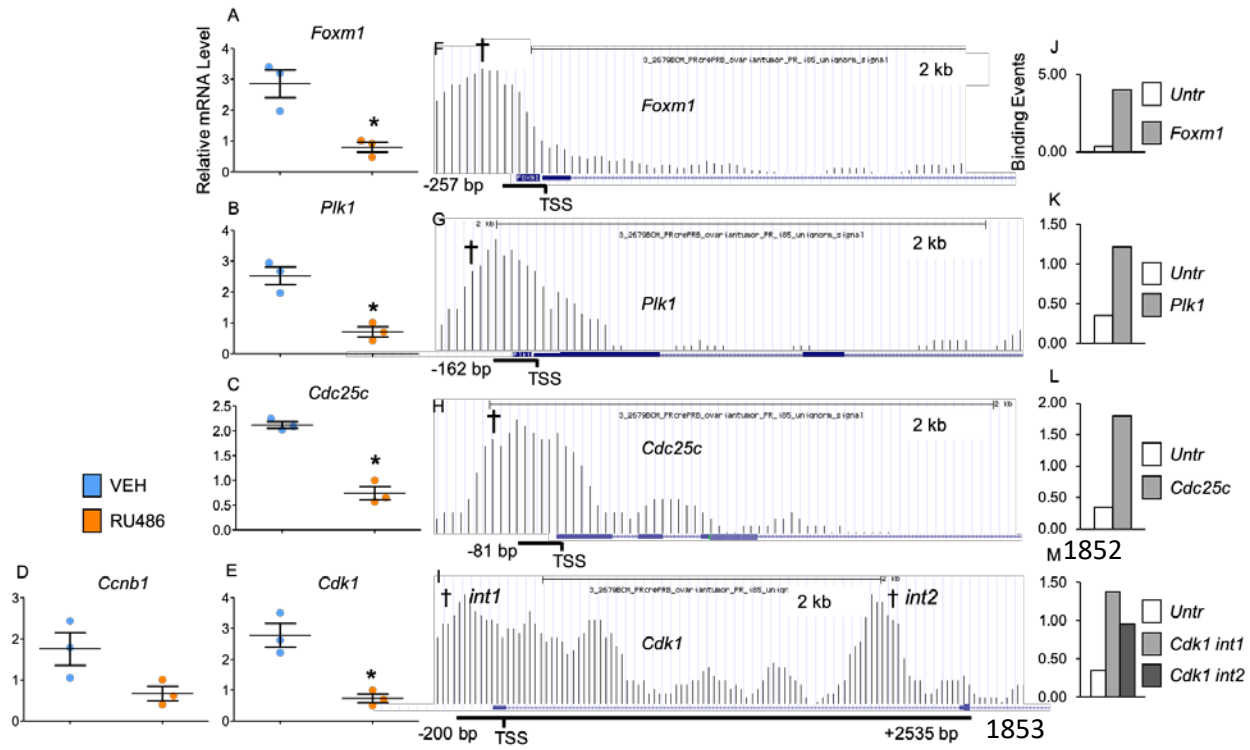

Supplemental Figure 14: PGRB promotes the cell cycle through direct regulation of genes necessary for the G2/M transition. Relative message levels for (A) *Foxm1*, (B) *Plk1*, (C) *Cdc25c*, (D) *Ccnb1*, and (E) *Cdk1*. (F-I) Graphical description of the PGR binding events for (F) *Foxm1*, (G) *Plk1*, (H) *Cdc25c*, and (I) *Cdk1* with validated binding intervals indicated by † and distances reported from transcription start site (TSS). (J-M) ChIP-qPCR validation results of binding events indicated with † described in (F-I) for *Foxm1* (J), *Plk1* (K), *Cdc25c* (L), and *Cdk1* (M). Y-axis represents the number of binding events detected per 1000 cells in the untranslated region versus interval of interest. Error bars indicate the standard deviation of averaged binding occurrences. Student's t-test was used to determine significance. *denotes significance with a p-value ≤ 0.05.

Age	Unilateral	Bilateral
23 weeks	2	0
28 weeks	4	2
33 weeks	7	1

Supplemental Table 1: Bilateral and unilateral tumors occur in $Pgr^{cre/+}mPgrB^{LsL/+}$ mice. n=16 mice.

Ingenuity Canonical Pathways	-log(p-value)	z-score	Molecules
Acute Phase Response Signaling	3.3	2.694	MAP2K6,IL6ST,FN1,APOH,PIK3R1,HRAS,SERPINA3,CP,FGG,MBL2,JUN,NFKBIA,ITIH4,RBP2,MRAS,AKT3,FGB,OSMR,LBP,TNFRSF1B,IL1RAP,C3,RRAS,IL6R,SERPINF1,MAPK8,C5,FOS,IL18,HP,APOA1,RRAS2,TF,PTPN11,CRP,PIK3CB,FGA,A2M
IL-8 Signaling	6.12	1.697	PRKD1,RND2,RRAS,FGFR1,RAC1,HBEGF,FGFR2,MMP2,MYL9,BCL2L1,ARRB2,CCND2,RHOQ,PTPN11,IRS1,PIK3R6,MAPK10,ANGPT2,PTK2B,PDGFC,EIF4EBP1,BCL2,JUN,KL,AKT3,FLT1,RHOC,MAPK8,IRAK3,CSTB,PLD4,ITGB2,FOS,RRAS2,PIK3CB,KDR,IRAK4,PRKCB
PI3K/AKT Signaling	1.28	2.236	TSC1,GAB2,JAK1,YWHAH,RRAS,PPP2R2A,PIK3R1,HRAS,MDM2,CCND1,EIF4EBP1,BCL2,BCL2L1,RRAS2,NFKBIA,FOXO1,PPM1L,MRAS,AKT3,PIK3CB,GSK3B,ITGA4,THEM4
CXCR4 Signaling	5.35	1.441	PIK3R1,HRAS,GNA14,BCAR1,FGFR3,GNB1,ROCK2,JUN,RHOB,KL,ADCY5,MRAS,AKT3,PRKD1,GNG12,RND2,ADCY2,PAK6,RRAS,RHOC,CXCR4,MYLPF,FGFR1,RAC1,ADCY6,MAPK8,FGFR2,ITPR1,MYL9,ADCY9,FOS,RRAS2,RHOQ,PAK3,PTPN11,IRS1,ITPR3,LYN,MAPK10,PIK3R6,PIK3CB,ELMO1,PRKCB
Cyclins and Cell Cycle Regulation	2.22	1.604	CCNE2,HDAC4,HDAC2,HDAC8,PPP2R2A,WEE1,CCND1,CDK1,SKP2,E2F6,CCNE1,CDKN2D,CCND2,PPM1L,E2F7,E2F5,TGFB2,GSK3B,E2F8
Macropinocytosis Signaling	4.68	1.606	RRAS,PDGFA,FGFR1,PIK3R1,RAC1,HRAS,FGFR2,RAB34,PDGFC,CSF1R,ITGB3,FGFR3,ITGB2,RRAS2,PTPN11,CSF1,KL,IRS1,PIK3R6,MRAS,CD14,PIK3CB,PDGFD,PRKD1,PRKCB
Ephrin Receptor Signaling	2.49	1.177	RAP1B,FYN,RAPGEF1,ITSN1,PDGFA,PTPN13,HRAS,EPHA4,LIMK2,GNA14,BCAR1,PDGFC,GRINA,ROCK2,GNB1,EPHB6,VEGFA,EFNB2,EFNA5,MRAS,AKT3,GNG12,ITGA4,GRIN2B,NGEF,PAK6,RRAS,CXCR4,ARHGEF15,CREBBP,RAC1,ATF2,RRAS2,PTPN11,PAK3,PDGFD

Supplemental Table 2: Canonical pathways are altered in 23-week-old neoplastic $Pgr^{cre/+}mPgrB^{LsL/+}$ mouse ovaries. Ingenuity Pathway Analysis was utilized to obtain the list of top canonical pathways from the RNA microarray performed on 23-week-old, neoplastic $Pgr^{cre/+}mPgrB^{LsL/+}$ mouse ovarian tumor tissue.

Ingenuity Canonical Pathways	-log(p-value)	Ratio	Molecules
Mitotic Roles of Polo-Like Kinase	5.93E00	2.3E-01	KIF23,PRC1,CDC20,KIF11,CDC25C,PLK3,CDC7,RAD21,STAG2,PLK4,PLK1,CDK1,CCNB1,FBXO5
Role of BRCA1 in DNA Damage Response	4.81E00	1.87E-01	FANCC,BRE,E2F1,BARD1,SMARCE1,FANCM,BRIP1,BLM,TOPBP1,FANCA,RBL1,RAD51,RFC4,PLK1
Cell Cycle Control of Chromosomal Replication	4.62E00	3.08E-01	CDC7,MCM2,ORC6,MCM6,CDT1,DBF4,MCM5,CDC6
Hereditary Breast Cancer Signaling	4.03E00	1.4E-01	FANCC,PALB2,MRAS,E2F1,BARD1,SMARCE1,FANCM,H2AFX,CDC25C,BLM,PMS2,CCND1,FANCA,RAD51,RFC4,CDK1,CCNB1
Estrogen-mediated S-phase Entry	3.94E00	2.92E-01	CCNE1,CCND1,SKP2,E2F1,CCNA2,RBL1,CDK1
Pancreatic Adenocarcinoma Signaling	3.85E00	1.47E-01	TGFA,HBEGF,TGFB3,NOTCH1,BIRC5,E2F1,RALGDS,RELA,SMAD3,CCND1,CCNE1,ERBB2,MDM2,BCL2L1,RAD51
Cell Cycle: G1/S Checkpoint Regulation	3.18E00	1.67E-01	TGFB3,CCNE1,CDKN2D,SMAD3,CCND1,SKP2,E2F1,MDM2,RBL1,MAX

Supplemental Table 3: PGR causes many changes in multiple canonical pathways involved in cell proliferation and cancer. Top canonical pathway list for differentially regulated genes between placebo and RU486 acute treatment in the RNA microarray.

Categories	p-Value	# Mols
Embryonic Development, Organismal Survival	1.35E-10	28
Cell Cycle	8.44E-08	19
Cell Cycle, DNA Replication, Recombination, and Repair	3.67E-07	15
DNA Replication, Recombination, and Repair	6.22E-07	17
Cell Cycle, Cellular Assembly and Organization, DNA Replication, Recombination, and Repair	7.47E-07	7
Cancer, Organismal Injury and Abnormalities, Respiratory Disease	2.55E-06	27
Cell Death and Survival	2.69E-06	120
Cellular Assembly and Organization	3.33E-06	7
Cellular Compromise, DNA Replication, Recombination, and Repair	6.79E-06	10
Cancer, Organismal Injury and Abnormalities	6.86E-06	48

Supplemental Table 4: PGR transcriptionally controls multiple canonical pathways involved in cell proliferation and cancer. Top biological function gene list from Ingenuity Pathway Analysis for the tumor microarray overlapped with the PGR ovarian tumor ChIP-seq analysis. #Mols=number of molecules, p-Value=p-value based on the Ingenuity Pathway Analysis algorithm for analyzing enrichment in a pathway.

Gene Name (species)	SYBR Primer Sequence
Cdc25c F (Mus musculus)	TTGCAAAGCGTAGCACATCTG
Cdc25c R (Mus musculus)	AAGGACCCGCGTCAATCA
Plk1 F (Mus musculus)	CCCGCTGGCGAAAGAAATTC
Plk1 R (Mus musculus)	CATTTGGCGAAGCCTCCTTTA
Ptgs1 F (Mus musculus)	TTGCACATCCATCCACTCCC
Ptgs1 R (Mus musculus)	AATTCCGAAGCCAGGTCCAG
Ptgs2 F (Mus musculus)	TTCAACACACTCTATCACTGGC
Ptgs2 R (Mus musculus)	AGAAGCGTTTGCGGTACTCAT
Gata4 F (Mus musculus)	CCCTACCCAGCCTACATGG
Gata4 R (Mus musculus)	ACATATCGAGATTGGGGTGTCT
Foxl2 F (Mus musculus)	ACAACACCGGAGAAACCAGAC
Foxl2 R (Mus musculus)	CGTAGAACGGGAACTTGGCTA
Inhbb F (Mus musculus)	CTTCGTCTCTAATGAAGGCAACC
Inhbb R (Mus musculus)	CTCCACCACATTCCACCTGTC
Foxo1 F (Mus musculus)	AGTGGATGGTGAAGAGCGTG
Foxo1 R (Mus musculus)	GAAGGGACAGATTGTGGCGA
Pgr F (Mus musculus)	CTCCGGGACCGAACAGAGT
Pgr R (Mus musculus)	ACAACAACCCTTTGGTAGCAG
Esr1 F (Mus musculus)	AAGTGTTACGAAGTGGGCATGA
Esr1 R (Mus musculus)	CTCTCTGACGCTTGTGCTTCAA
Esr2 F (Mus musculus)	CTGTTACTAGTCCAAGCGCCA
Esr2 R (Mus musculus)	CCCAGATGCATAATCACTGCA
Gene Name (species)	Applied Biosystems Taqman Cat #
Hand2 (Mus musculus)	Mm00439247_m1
Ccnd1 (Mus musculus)	Mm00432359_m1
Foxm1 (Mus musculus)	Mm00514924_m1
Cdk1 (Mus musculus)	Mm00772471_m1
Ccnb1 (Mus musculus)	Mm00838401_g1

Supplemental Table 5: Complete list of SYBR primer sequences and Applied Biosystems Taqman probe catalog numbers.